Journal of Alloys and Compounds 509 (2011) 3299–3305

Contents lists available at ScienceDirect

Journal of Alloys and Compounds

journal homepage: www.elsevier.com/locate/jallcom

Microstructures and mechanical properties of the extruded Mg-4Y-2Gd-*x*Zn-0.4Zr alloys

Ke Liu[a,*], Jian Meng[b,*]

[a] School of Materials Science and Engineering Beijing University of Technology, Beijing 100124, PR China
[b] State Key Laboratory of Rare Earth Resources Utilization, Changchun Institute of Applied Chemistry, Chinese Academy of Sciences, Changchun, 130022, PR China

ARTICLE INFO

Article history:
Received 8 February 2010
Received in revised form 2 December 2010
Accepted 3 December 2010
Available online 13 December 2010

Keywords:
Magnesium alloys
Age hardening behavior
Mechanical properties

ABSTRACT

Microstructures and mechanical properties of the Mg-4Y-2Gd-0.4Zr alloy with Zn additions have been investigated. The investigation suggests that the mechanical properties of the alloys have been greatly improved after hot extrusion due to the refinement of microstructures, especially the elongations. The extruded Mg-4Y-2Gd-1.0Zn-0.4Zr alloy displays excellent tensile properties. The ultimate tensile strength and the yield tensile strength are 291 and 228 MPa, respectively, with an elongation of 28%. The additions of Zn have an obvious effect on refining microstructure of the extruded alloys, and the vicker hardness increases with increasing Zn additions. The age hardening responses of the extruded alloys have been investigated at 220 °C. These alloys display unobvious ageing hardness responses.

1. Introduction

Magnesium alloys have been received a great attention as light-weight structure materials because of specific strength, high stiffness, good damping capacity and easy-recycling and so on [1]. However, the present commercial magnesium alloys display disappointing mechanical properties. Zn is often added to improve both the yield tensile strength (YTS) and the ductility of the wrought magnesium alloys [2–7]. Kawamura et al. [8] have developed a RS P/M Mg-1Zn-2Y (at.%) alloy, and this alloy shows excellent mechanical properties. The YTS and elongation are 610 MPa and 5%, respectively. Recently, Homma et al. [9] reported that the Mg-1.8Gd-1.8Y-0.7Zn-0.2Zr alloy fabricated by conventional hot extrusion exhibited a highest ultimate tensile strength (UTS) of 542 MPa with an elongation of 8.0%.

The Zn additions lead to a formation of a long periodic stacking (LPS) structure, which has a great effect on enhancing the mechanical properties of these magnesium alloys [10–14]. It has been reported that these LPS structures prevented the growth of $\{1\,0\,\bar{1}\,2\}$ deformation twins [11]. The LPS structure has been observed in the Mg-Zn-RE (RE containing Y, Gd, Ce, Sm, La and La(MM)), and the formation of this LPS structure is a universal phenomenon [15–18]. In our previous work, the LPS structure had been observed in the Mg-Zn-Y-Gd-Zr and Mg-Zn-Gd-Zr series alloys, and these investigations suggested that this structure has a great effect on improving mechanical properties, including tensile strength and elongation [4,5,10,12].

In this investigation, the microstructures and mechanical properties of the Mg-4Y-2Gd-*x*Zn-0.4Zr alloys (wt.%) (x = 0, 0.5 1.0, 1.5, 2.0 and are identified by alloys A, B, C, D and E, respectively) have been investigated. These alloys in the extruded condition were aged at 220 °C, and the precipitates observed after peak ageing have been investigated.

2. Experimental procedures

The alloy ingots with nominal compositions of Mg-4Y-2Gd-*x*Zn-0.4Zr were produced from high-purity Mg (99.5%), high-purity Zn (>99.9%), Mg-20Y (wt.%), Mg-25Gd (wt.%) and Mg-35Zr (wt.%) master alloys in an electric resistance furnace at about 750 °C. The mild steel crucible was filled with a protective atmosphere. At about 730 °C, the melts were poured into an iron mold with a diameter of 90 mm. Specimens, which were used for the cast research were cut from the cylinder-shaped ingots. Parts of them were made into rectangular tensile specimens of 15 mm in gauge length, 3 mm in width and 1.5 mm in thickness, and the remaining was used for other investigations. The cylinder-shaped ingots homogenized at 500 °C for 8 h were milled into a diameter of 82 mm, and then were extruded into rods in the extrusion ratio about 16.8 at 380 °C. Some rods were directly aged at 220 °C in order to investigate the age hardening behaviors with time. The tensile specimens of the alloys in as-extruded and peak-ageing conditions were also machined into the same geometry as the cast samples.

Tensile tests were carried out on a uniaxial tensile testing machine at primary strain rate of 1 mm/min. The tensile axis was aligned parallel to the extrusion direction. Vickers hardness was measured by a hardness tester with a load of 100 or 15 g, a dwelling time of 15 s and 20 measurements were collected for each sample. The microstructures of the alloys were observed by an optical microscope

* Corresponding authors. Tel.: +86 10 67392423; fax: +86 10 67392423.
E-mail address: lk@bjut.edu.cn (K. Liu).

0925-8388/$ – see front matter © 2010 Elsevier B.V. All rights reserved.
doi:10.1016/j.jallcom.2010.12.015

(OM), scanning electron microscope (SEM) with an energy dispersive spectroscope (EDS) and transmission electron microscope (TEM). The grain sizes of the alloys were measured via using an average linear intercept method. The samples were mechanical polishing and etching in a solution of 2.1 g picric acid, 5 ml acetic acid, 35 ml ethanol and 5 ml H_2O. Samples for TEM were prepared with an argon ion milling technique. Phase analysis went along with an X-ray diffraction (XRD).

3. Experimental results

3.1. Microstructures of the cast alloys A, B, C and E

Fig. 1 shows the microstructures of the cast alloys A, B, C and E. It is suggested that the Zn additions lead to a formation of a kind

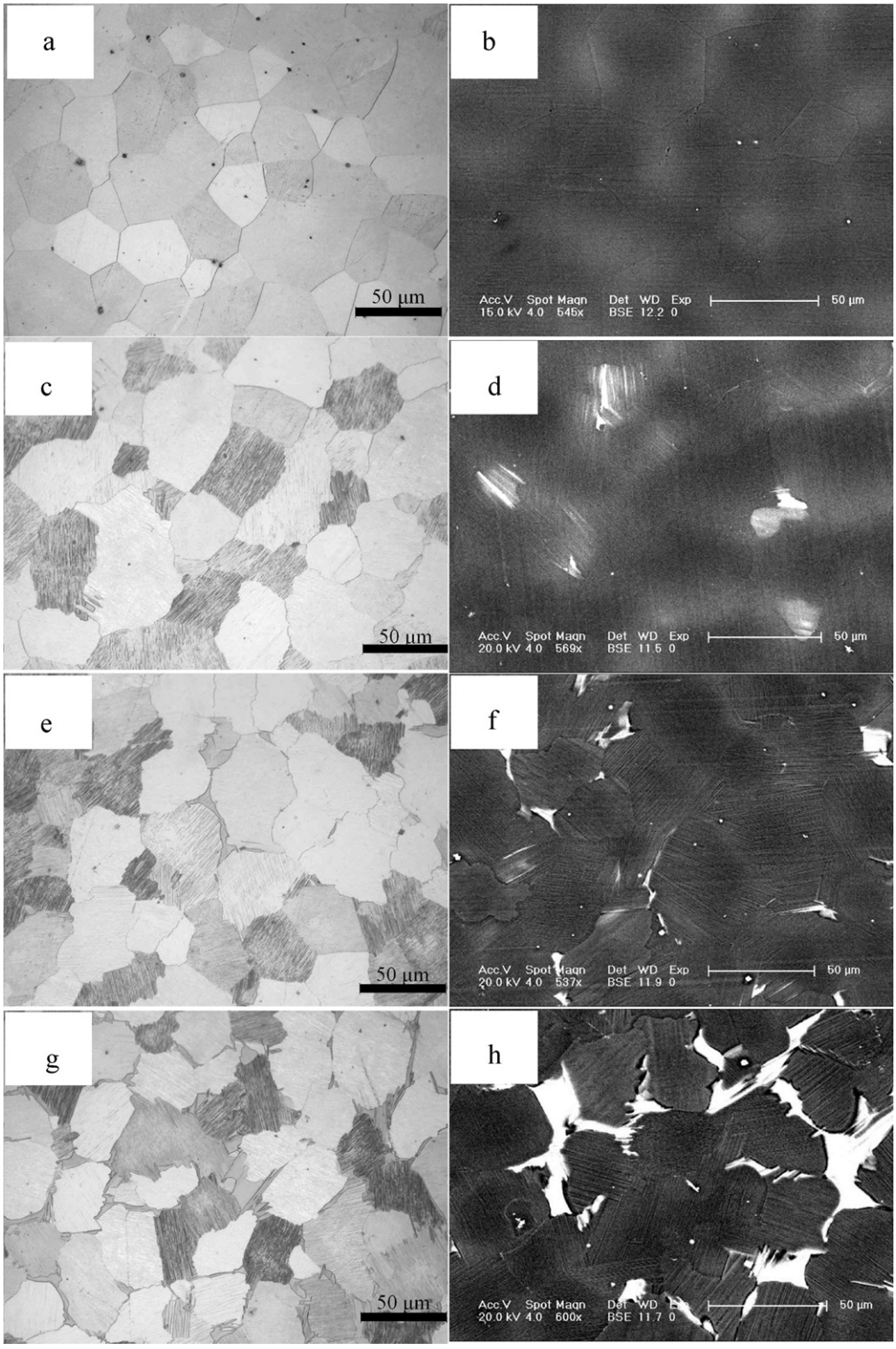

Fig. 1. OM and SEM images of the cast alloys: (a and b) alloy A, (c and d) alloy B, (e and f) alloy C and (g and h) alloy E.

of lamellar phase and the volume fraction of this phase increases with increasing Zn additions. The average grain sizes of the alloys A, B, C and E are 35.98, 32.60, 30.37 and 32.59 μm, respectively.

Fig. 2 shows the SEM image and corresponding EDS results obtained from the lamellar phase of the cast alloy B. It is observed that the lamellar phase is mainly located at the grain boundaries. However, it is also observed the presence of this lamellar phase within the matrix. The EDS result shows that the composition of this phase is about Mg-3.44 RE-2.11 Zn (at.%). However, this chemical composition is different from that of the LPS structure obtained from both the cast Mg-7Y-4Gd-*x*Zn-0.4Zr alloys and the cast Mg-5Y-4Gd-*x*Zn-0.4Zr alloys [4,10].

In order to investigate the microstructure of the LPS structure observed in the cast Mg-4Y-2Gd-0.5Zn-0.4Zr alloy, the TEM observation has been conducted, as shown in Fig. 3. Fig. 3a shows the microstructure of the LPS structure. This phase is located at the grain boundaries. High-resolution electron microscopy (HREM) has

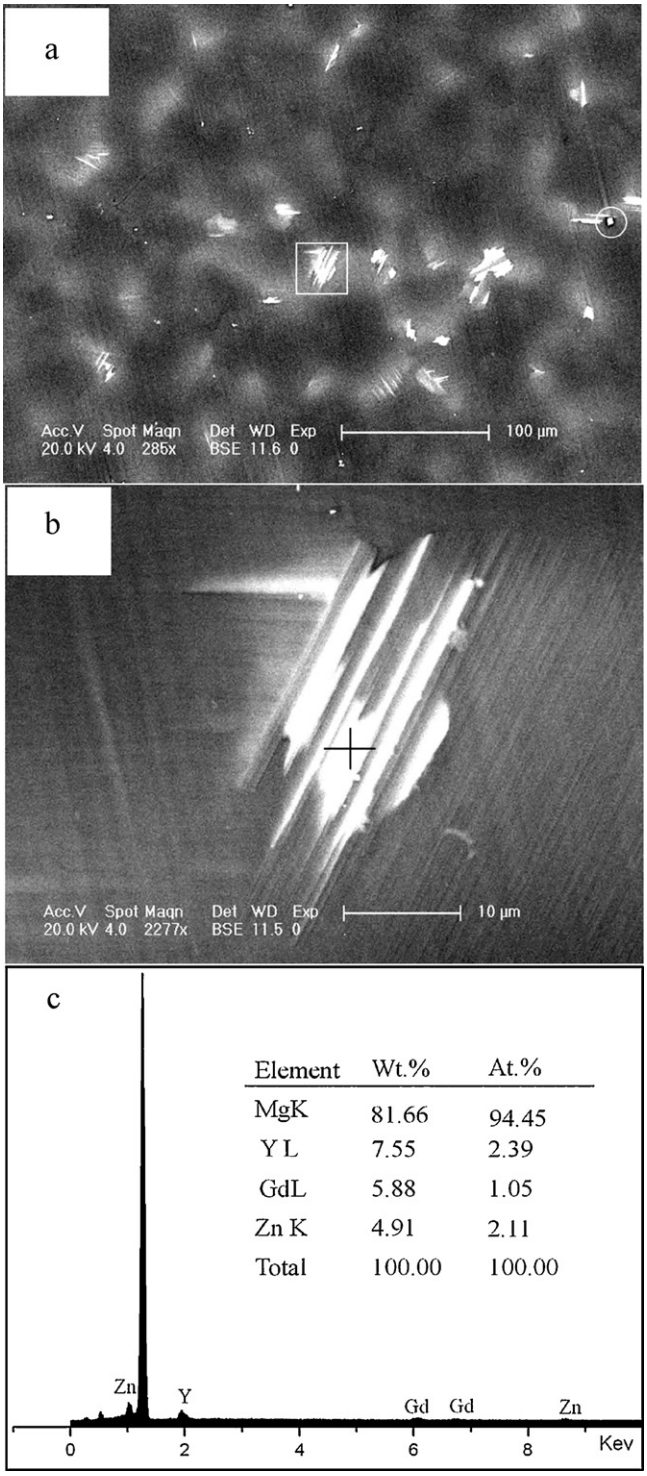

Fig. 2. SEM images and EDS result of the cast alloy B: (a) SEM image of this alloy, (b) SEM image at a high magnification obtained from the LPS structure and (c) EDS result of the LPS structure.

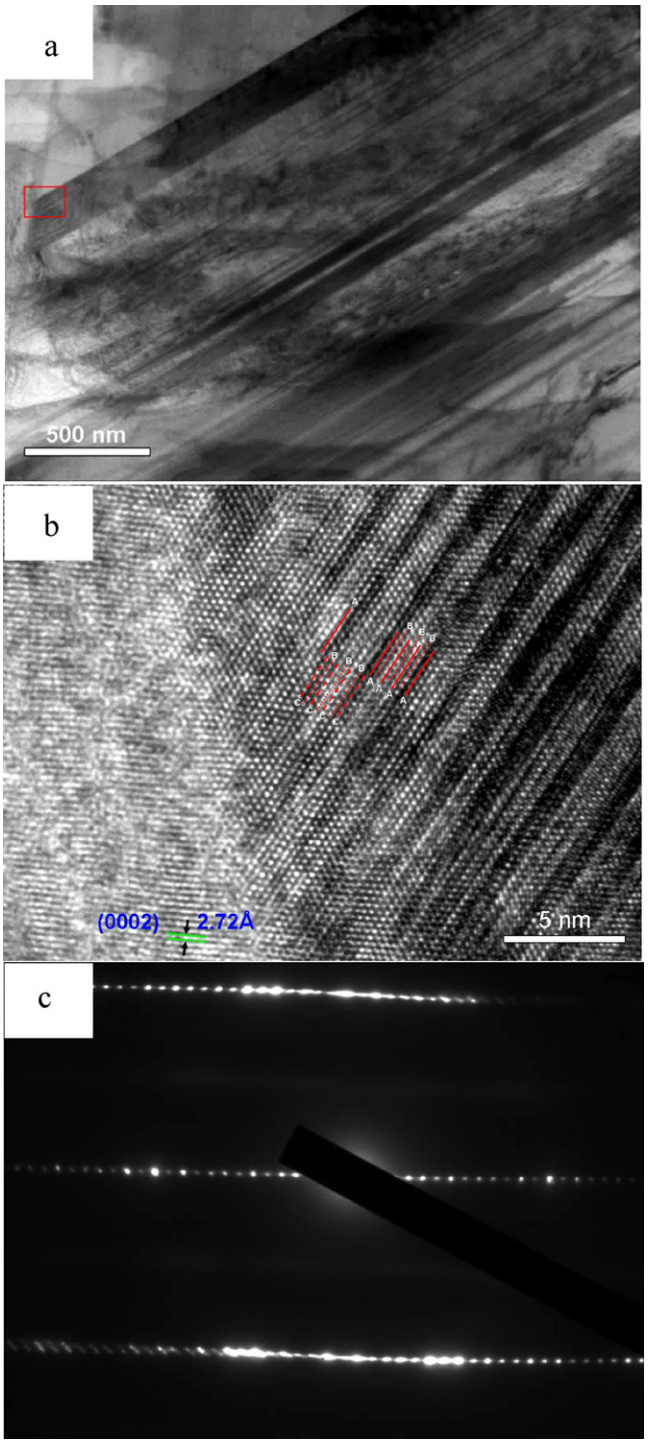

Fig. 3. TEM images and corresponding SAED pattern of the cast alloy B: (a) TEM image of the LPS structure, (b) HREM image of the 14H LPS structure and (c) corresponding SAED pattern obtained from the LPS structure.

been taken from this precipitate, as shown in Fig. 3b. The HREM image shows a stacking sequence of ABABABACBCBCBC, and it suggests that this phase has a 14H-type structure. The SAED pattern has been obtained from this phase and confirmed the existence of the 14H structure.

3.2. Microstructures of the extruded alloys A, B, C and E

The microstructures of the extruded alloys A, B, C and E have been shown in Fig. 4. These OM images show that the microstructures have been refined after hot extrusion. The average grain sizes

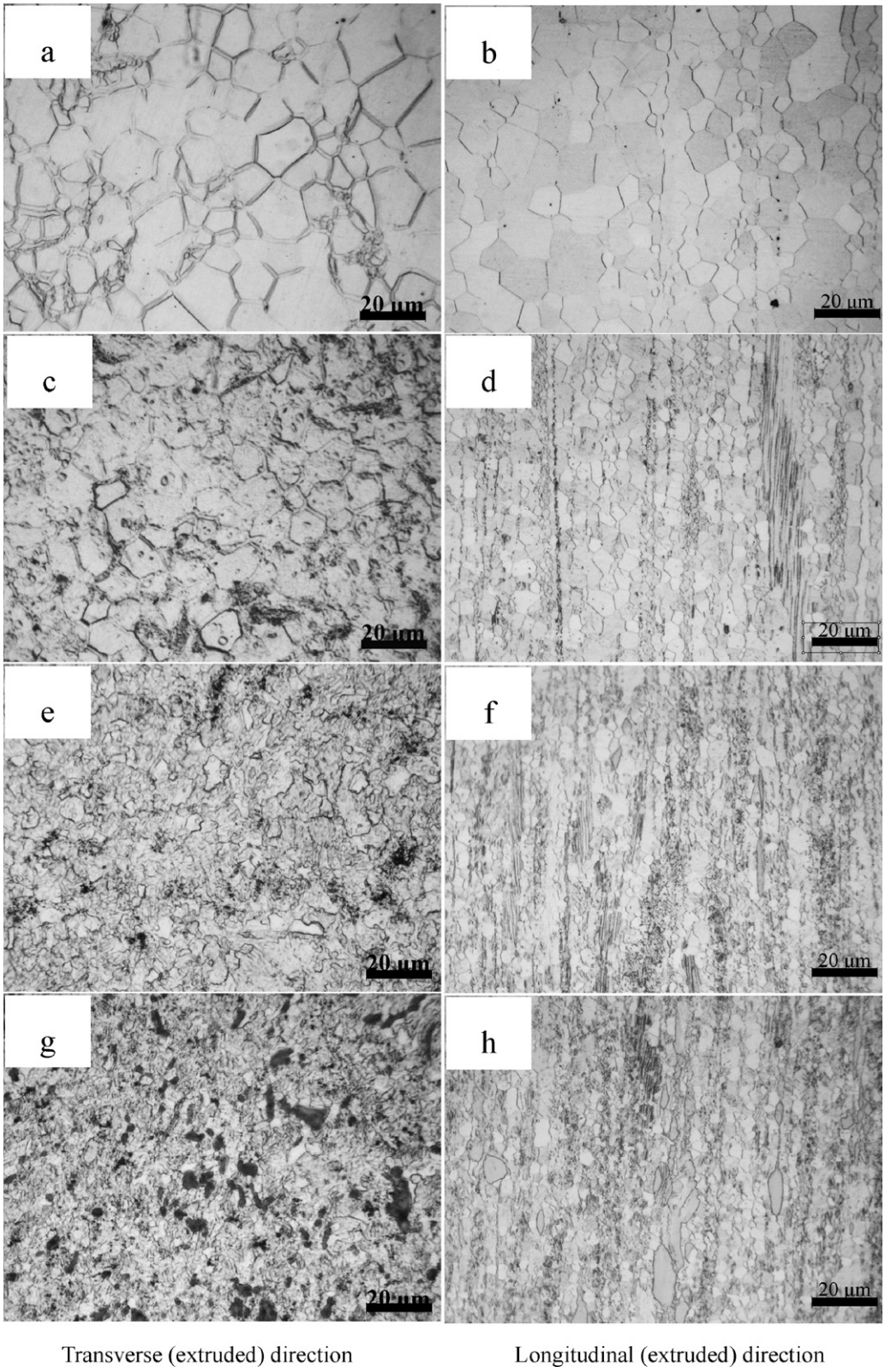

Fig. 4. OM images of the extruded alloys: (a and b) alloy A, (c and d) alloy B, (e and f) alloy C and (g and h) alloy E.

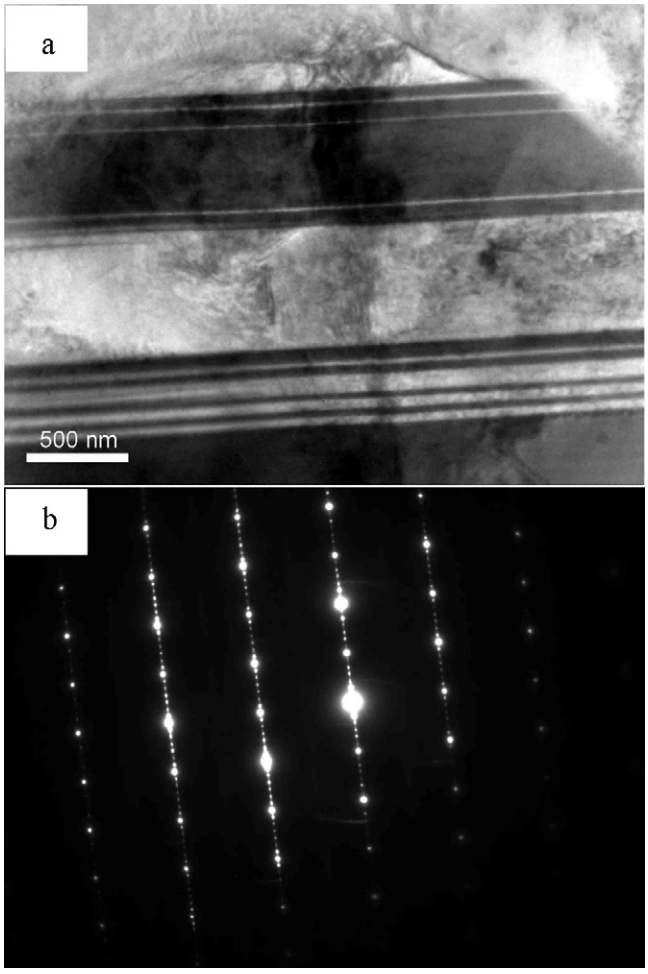

Fig. 5. TEM image and corresponding SAED pattern of the extruded alloys B: (a) TEM image of the LPS structure and (b) corresponding SAED pattern obtained from this LPS structure.

of the alloys A, B, C and E are 14.23, 12.47, 8.45 and 5.14 μm, respectively. Furthermore, it is found that the dynamic recrystallization (DRX) occurred, as shown in Fig. 4b, d, f and h. DRX has an important effect on refining the microstructures [19–21]. Secondary phases were broken and then were distributed along the extrusion direction. These secondary phases play an important role in limiting the growth of the recrystallized grains [4].

Fig. 5 shows the TEM image and corresponding SAED pattern of the LPS structure observed in the extruded alloy B. The SAED pattern shows that there are 13 diffraction intensity maxima between $(0\,0\,0\,1)_\alpha$ and $(0\,0\,0\,2)_\alpha$. It indicates that a LPS structure with a 14 basal plane periodicity. It is shown that this phase has an identical structure with that observed in the cast alloy B.

3.3. Hardness of the LPS structures in the cast and extruded alloys

The hardness of the lamellar phase observed in both the cast alloy and the extruded alloy has been investigated. This Vickers hardness was collected with a load of 15 g. The hardness of the LPS structure obtained from the cast alloys B, C, D and E are 84.57, 86.86, 88.39 and 88.96 VHN, respectively. These values are similar with each other. Furthermore, the values of the hardness of this structure collected from these extruded alloys B, C, D and E are 84.68, 87.64, 87.92 and 86.41 VHN, respectively. It is found that the hardness of these LPS structures is the same in either the cast alloy or the extruded alloy.

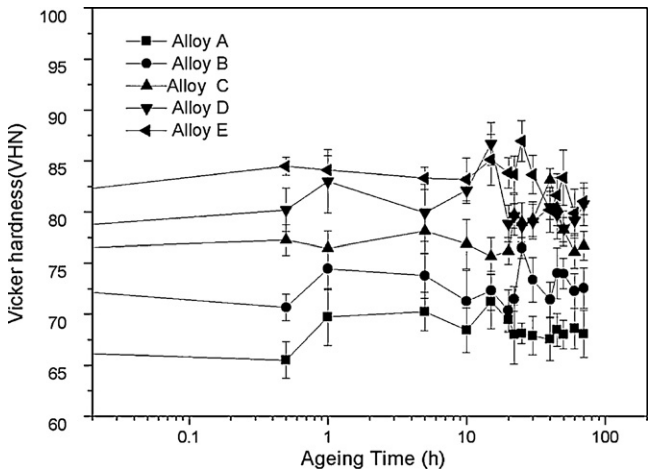

Fig. 6. Age hardening behaviors of the extruded alloys A, B, C, D and E.

3.4. Ageing behaviors and microstructures of the peak-ageing alloys

Fig. 6 shows the ageing behaviors of the extruded alloys A, B, C, D and E at 220 °C. It is suggested that the ageing behaviors of these alloys are not obvious. The Vickers hardness was measured with a load of 100 g. The hardness of these alloys increases with increasing Zn additions. However, the hardness has no obvious improvement during ageing process. The values of the peak-ageing hardness of the alloys A, B, C, D and E are 70.26, 76.48, 83.13, 86.67 and 86.96 VHN, respectively. The reduction of the RE content directly leads to a big fall in peak-ageing hardness compared with our previous work [4–5,10,12].

Fig. 7 shows the TEM images and the corresponding SAED patterns obtained from the peak-ageing samples of the alloys B and E. Fig. 7a shows the phase with a 14H-type structure precipitated at the matrixes observed from the peak-ageing alloy B. Because the extrusion temperature was 380 °C, this LPS structure was formed at this temperature. The precipitation of this phase has no contribution to the age hardening response of the alloy B. The TEM observation of the peak-ageing specimen of the alloy E shows that two types of phase coexist together throughout the α-Mg matrix. One is the β′ phase with an ellipsoidal morphology which is identified by "A" in Fig. 7b, the other is $MgZn_2$ phase distributed randomly in the matrix with a rod morphology which is stressed by "B" in Fig. 7b. In fact, the LPS structure precipitated at matrix in the alloy E has been observed, which is not shown. Because the number of the β′ phase is small and the size is large, it is considered that this phase is formed during the holding time at the extrusion temperature rather than during the ageing at 220 °C. The amount of such precipitates is so low that their contribution to the total strength of the alloys should be negligible. However, the high content of Zn (alloy E) leads to the abundant binary Mg–Zn phase forming during ageing at 220 °C. The precipitates of the $MgZn_2$ phase are mainly responsible for the improvement of the hardness after peak ageing.

3.5. Mechanical properties

Table 1 shows the tensile properties of the cast alloys A, B, C, D and E. The better ultimate tensile strength (UTS) is observed in the alloy B, and the value of the UTS is 217 MPa with an elongation of 15%. It is concluded that the addition of 0.5 wt.% Zn leads to improved mechanical properties of the cast Mg-4Y-2Gd-0.4Zr alloy. However, the values of the yield tensile strength (YTS) of the cast alloys B, C and D are similar. It is suggested that a further increase in the Zn content does not imply a higher YTS in the cast alloys. In

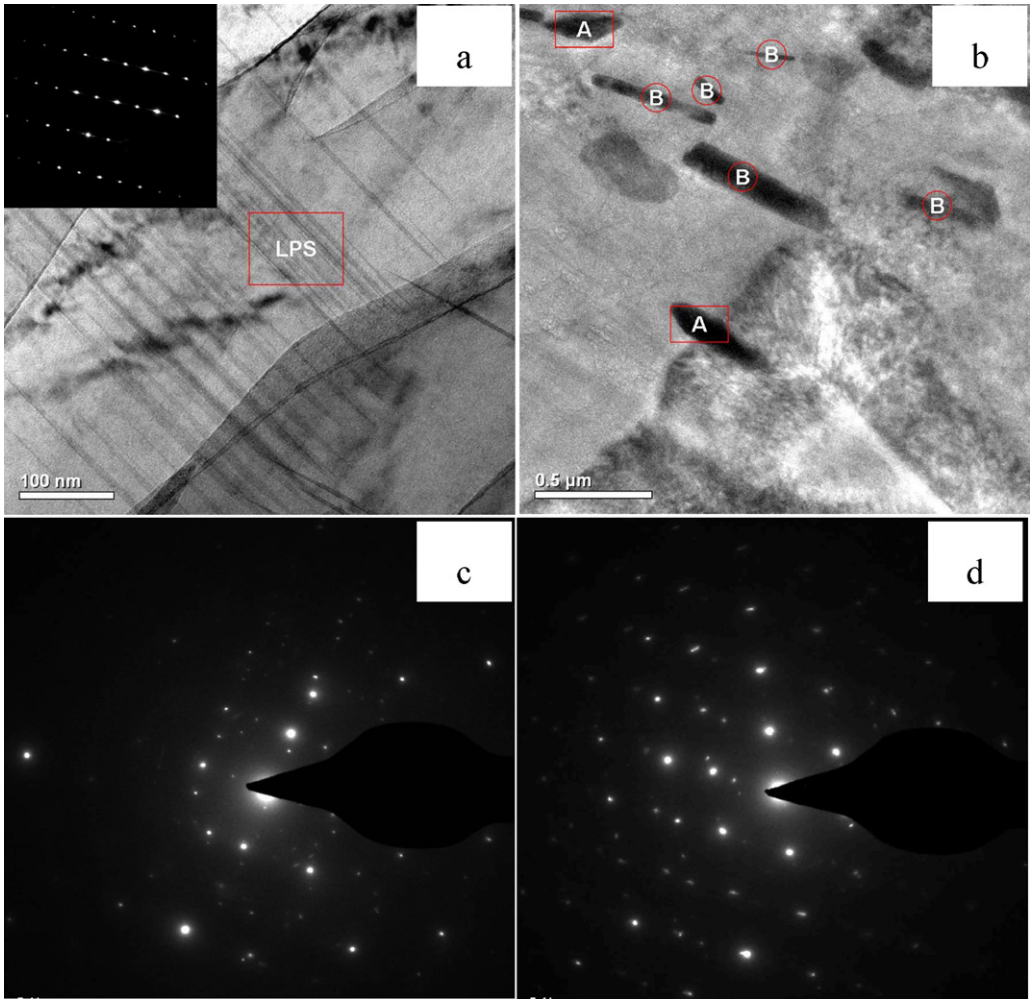

Fig. 7. TEM images of the peak-ageing alloys B and E: (a) TEM image and corresponding SAED pattern of the alloy B, (b) TEM image of the β′ phase and the $MgZn_2$ phase obtained from the alloy E, (c) and (d) corresponding SAED patterns of the β′ phase and $MgZn_2$ phase, respectively.

Table 1
Tensile properties of the cast alloys at room temperature.

Alloys	UTS (MPa)	TYS (MPa)	Elongation (%)
A	175	93	8.0
B	217	103	15
C	202	108	12
D	194	110	7.5
E	192	90	8.5

particular, the Zn addition up to 2.0 wt.% results in a big fall in the YTS due to the LPS structure getting coarse. The value of the YTS of the cast alloy E is 90 MPa with an elongation of 8.5%.

Table 2 shows the mechanical properties of the extruded alloys. It is suggested that the mechanical properties of the alloys are greatly improved after hot extrusion. Moreover, the tensile strength of the extruded alloys is improved gradually with an increase in the Zn content. The alloy E exhibits the highest tensile strength mostly due to a higher volume fraction of the LPS structure and refined microstructure. The values of the UTS and YTS of the extruded alloy E are 318 and 240 MPa, respectively, and the elongation is 20%. In addition, the plasticity decreases with more Zn additions. However, compared with the mechanical properties of the Mg-5Y-4Gd-*x*Zn-0.4Zr (wt.%) (x = 0, 0.5, 1.0, 1.5 and 2.0) alloys in our previous work, these extruded alloys still display a higher ductility but lower strengths [10].

Table 3 shows the tensile properties of the peak-ageing alloys. It is found that the tensile strengths of these alloys have no distinct improvement. The alloy E shows the best tensile strength. The values of the UTS and YTS are 328 and 261 MPa, respectively, and the value of the elongation is 17%. It is suggested that lower content of the RE leads to the inferior ageing behaviors in these alloys.

Table 2
Tensile properties of the extruded alloys at room temperature.

Alloys	UTS (MPa)	TYS (MPa)	Elongation (%)
A	222	138	30
B	260	182	28
C	291	228	27
D	300	232	25
E	318	240	20

Table 3
Tensile properties of the alloys in the peak-ageing condition testing at room temperature.

Alloys	UTS (MPa)	TYS (MPa)	Elongation (%)
A	224	146	27
B	263	187	27
C	301	242	25
D	314	243	22
E	328	261	17

4. Discussion

The microstructures and mechanical properties of the Mg-4Y-2Gd-*x*Zn-0.4Zr (wt.%) (x = 0, 0.5, 1.0, 1.5 and 2.0) alloys have been investigated. The 14H LPS structure has been observed in the cast, the extruded and the peak-ageing alloys. The LPS structure is a universal phase in the Mg-RE-Zn alloys [15]. Furthermore, five types of this structure have been observed, i.e. 6H, 10H, 14H, 18R and 24R [6,22–25]. The 18R structure formed during solidification with fast cooling rate that reduced the energy barrier for forming the 18R LPS structure [24,26,27]. However, Itoi et al. [28] reported that 18R LPS structure was transformed to a 14H LPS structure after annealing at 500 °C for 5 h. It is concluded that the 14H LPS structure is more stable compared with the 18R LPS structure. Datta et al. [29] reported that the formation energy of the 14H LPS structure was close to the energy of the hcp structure, and the 14H LPS structure is more stable than the 6H LPS structure. In this investigation, the 14H LPS structure has been observed in both the cast and the extruded Mg-4Y-2Gd-0.4Zr alloys with Zn containing.

In this investigation, the results agree with previous literature on Mg-Zn-Gd, Mg-Zn-Y, Mg-Zn-Y-Gd alloys, and the additions of Zn lead to a formation of the LPS structure. The LPS structure as a strengthening phase formed during solidification, and the volume fraction of this structure increases with increasing Zn addition. This structure was considered as a strengthening phase in the magnesium alloys by Kawamura and Abe. Chino et al. confirmed that the hardness was improved by the LPS structure by carrying out a microindentation test form the RS P/M material and pure magnesium. In this investigated alloys, the strength of the extruded Mg-4Y-2Gd-0.4Zr alloy is progressively increased with increasing the volume fraction of the LPS structure. It is further suggested that this LPS structure has a great effect on improving the mechanical properties of the magnesium alloys.

Although the additions of Zn played an important role in decreasing the solubility of RE in the matrix, the lower content of the RE in the matrix led to an unobvious peak-ageing hardness at 220 °C. So these peak-ageing alloys did not show high tensile strength but companying with good elongation. However, the $MgZn_2$ phase formed during ageing with increasing Zn additions up to 2.0 wt.%. It is considered that the ageing response of the alloy E is attributed to the presence of the the $MgZn_2$ phase.

5. Conclusions

In this article, the microstructures and the mechanical properties of these alloys A, B, C, D and E have been investigated. The below conclusions were obtained:

1. The LPS structure with a 14 basal plane periodicity has been observed in the alloys containing Zn. The LPS structure has an important effect on improving the tensile strength of the alloys.
2. These alloys with a lower content of RE showed inferior tensile strength and unconspicuous age hardening responses compared with both the Mg-7Y-4Gd-*x*Zn alloys and the Mg-5Y-4Gd-*x*Zn alloys. However, the elongations of the alloys in both the extruded and the peak-ageing conditions are better.
3. The Mg-4Y-2Gd-2.0Zn-0.4Zr alloy in the peak-ageing condition displays the best mechanical properties because of the precipitations of the $MgZn_2$ phase.

Acknowledgements

This project was supported by Hi-Tech Research and Development Program of China (2006AA03Z520), Chinese Academy of Sciences and Jilin Province and Baikov Institute of Metallurgy and Materials Science, Russian Academy of Sciences, Moscow, Russia.

References

[1] D.J. Li, X.Q. Zeng, J. Dong, C.Q. Zhai, W.J. Ding, J. Alloys Compd. 468 (2009) 164–169.
[2] Y. Gao, Q.D. Wang, J.H. Gu, Y. Zhao, Y. Tong, D.D. Yin, J. Alloys Compd. 477 (2009) 374–378.
[3] X.B. Liu, R.S. Chen, E.H. Han, J. Alloys Compd. 465 (2008) 232–238.
[4] K. Liu, J.H. Zhang, W. Sun, X. Qiu, H.Y. Lu, D.X. Tang, L.L. Rokhlin, F.M. Elkin, J. Meng, J. Mater. Sci. 44 (2009) 74–83.
[5] K. Liu, J.H. Zhang, D.X. Tang, L.L. Rokhlin, F.M. Elkin, J. Meng, Mater. Sci. Eng. A 505 (2009) 13–19.
[6] T. Honma, T. Ohkubo, S. Kamado, K. Hono, Acta Mater. 55 (2007) 4137–4150.
[7] K. Yamada, Y. Ohkubo, M. Shiono, H. Watanabe, S. Kamado, Y. Kojima, Mater. Trans. 47 (2006) 1066–1070.
[8] Y. Kawamura, K. Hayashi, A. Inoue, T. Masumoto, Mater. Trans JIM 42 (2001) 1172–1176.
[9] T. Homma, N. Kunito, S. Kamado, Scripta Mater. 61 (2009) 644–647.
[10] K. Liu, J.H. Zhang, G.H. SU, D.X. Tang, L.L. Rokhlin, F.M. Elkin, J. Meng, J. Alloys Compd. 481 (2009) 811–818.
[11] M. Matsuda, S. Ii, Y. Kawamura, Y. Ikuhara, M. Nishida, Mater. Sci. Eng. A 386 (2004) 447–452.
[12] K. Liu, J.H. Zhang, H.Y. Lu, D.X. Tang, L.L. Rokhlin, F.M. Elkin, J. Meng, Mater. Des. 31 (2009) 210–219.
[13] Y.M. Zhu, A.J. Morton, J.F. Nie, Acta Mater. 58 (2010) 2936–2947.
[14] D.D. Yin, Q.D. Wang, Y. Gao, C.J. Chen, J. Zheng, J. Alloys Compd. (2010), doi:10.1016/j.jallcom.2010.09.194.
[15] K. Amiya, T. Ohsuna, A. Inoue, Mater. Trans. 44 (2003) 2151–2156.
[16] P. Pérez, G. Garcés, P. Adeva, J. Alloys Compd. 491 (2009) 192–199.
[17] Y.J. Wu, X.Q. Zeng, D.L. Lin, L.M. Peng, W.J. Ding, J. Alloys Compd. 477 (2009) 193–197.
[18] Z.H. Huang, S.M. Liang, R.S. Chen, E.H. Han, J. Alloys Compd. 468 (2009) 170–178.
[19] T. Mohri, M. Mabuchi, N. Nakamura, T. Asahina, H. Iwasaki, T. Aizawa, K. Higashi, Mater. Sci. Eng. A 290 (2000) 139–144.
[20] Z. Yang, Y.C. Guo, J.P. Li, F. He, F. Xia, M.X. Liang, Mater. Sci. Eng. A 485 (2008) 487–491.
[21] J.C. Tan, M.J. Tan, Mater. Sci. Eng. A 339 (2003) 124–132.
[22] E. Abe, Y. Kawamura, K. Hayashi, A. Inoue, Acta Mater. 50 (2002) 3845–3857.
[23] M. Yamasaki, T. Anan, S. Yoshimoto, Y. Kawamura, Scripta Mater. 53 (2005) 799–803.
[24] Z.P. Luo, S.Q. Zhang, J. Mater. Sci. Lett. 19 (2000) 813–815.
[25] M. Matsuda, S. Ii, Y. Kawamura, Y. Ikuhara, M. Nishida, Mater. Sci. Eng. A 393 (2005) 269–274.
[26] M. Zhang, S.J. Zhu, G.L. Chen, B.F. Zhang, S.K. Guan, Found. Tech. 26 (2005) 983–985.
[27] J.Y. Liu, Z.Z. Zhang, M. Hua, L.Q. Ma, X.D. Shen, Found. Tech. 27 (2006) 258–262.
[28] T. Itoi, T. Seimiya, T. Seimiya, Y. Kawamura, M. Hirohashi, Scripta Mater. 51 (2004) 107–111.
[29] A. Datta, U.V. Waghmare, U. Ramamurty, Acta Mater. 56 (2008) 2531–2539.